Change Detection based on Bayes' Theorem for Intensity Wavelength-Resolution SAR Difference Images

Gabriel Luiz Espindola Pedro, Dimas Irion Alves, Diego da Silva de Medeiros,
Paulo Ricardo Branco da Silva, João Vitor Rosa Negri and Arthur Cadore Matuella Barcella

***Abstract*— Detecting concealed targets under foliage remains a significant challenge for wavelength-resolution synthetic aperture radar (SAR) systems. This paper proposes the usage of the bivariate Gamma distribution as a clutter model, shown to be a well-fitted distribution for intensity SAR difference images, on an noniterative Change Detection (CD) algorithm based on Bayes' Theorem. The results were compared by using ROC curves and a probability of detection of 98.94% at false alarm ratio of 1 per kilometer squared was achieved, outperforming previously used distributions in the literature.**

***Keywords*— CARABAS II, change detection, bivariate Gamma distribution, background statistics**

I. Introduction

Detecting concealed targets beneath vegetation is a persistent challenge for conventional imaging systems. Optical sensors, in particular, are highly susceptible to weather conditions. Synthetic Aperture Radar (SAR) systems mitigate the impact of weather on image formation. However, in traditional microwave SAR systems, foliage still interacts with the radar signal, making concealed-target detection difficult [1].

To address this issue, wavelength-resolution SAR systems operate at low frequencies, ensuring that the dominant scatterers correspond to the transmitted signal's wavelength, i.e., small scatterers will not add predominant interference on the reflected signal, thus penetrating vegetation and being able to detect targets under foliage [2]. Additionally, these systems are not significantly affected by the speckle noise phenomenon [3].

Due to the electromagnetic nature associated with SAR image formation, interpreting information in SAR images tends to be challenging for human analysts [4]. Because of this, target detection is usually done using automatic detection algorithms [4]. One category of algorithms often used for this task is change detection algorithms, which check for variations between two or more images [5], [6].

Considering the statistical behavior of SAR images, Change Detection (CD) methods are typically developed using statistical approaches. Some studies employ the Likelihood Ratio Test (LRT) [7], which evaluates the likelihood of the null hypothesis H_0, stating that the region under test consists of clutter, against the alternative hypothesis H_1, indicating the presence of a target. Other studies adopt an approach based on Bayes' Theorem, in an iterative and noniterative manner [6], [8], to perform detection by comparing the expected value of a pixel under the clutter model with the empirical value observed in the image.

Since clutter statistics can be modeled as following a known distribution, the performance of the CD method can be improved by identifying a distribution that more accurately represents the clutter behavior in these type of images. Additionally, by processing the images, their statistical properties change, making it possible to describe clutter behavior using different distributions [9].

In [6], it was shown that the Bivariate Rayleigh distribution can be used to model the clutter in incoherent wavelength-resolution SAR images, particularly in regions of interest for detection. Additionally, studies have demonstrated that the Bivariate Gamma distribution provides a good fit for intensity wavelength-resolution SAR difference images [9].

Considering that the Bayesian CD method developed by Alves et al. demonstrated superior performance compared to other approaches in the literature [8], and that it relies on an underlying clutter model, this paper focuses on applying the statistical model proposed in [9] within the CD framework of [8]. We adopt the non-iterative version of the CD method due to its lower computational complexity.

The remainder of this paper is organized as follows. Section II describes the characteristics of wavelength-resolution SAR images and the dataset used in the performance tests. Section III presents the change detection method used in this paper. Section IV demonstrates the results obtained for the change detection method with the currently studied models for the clutter-plus-noise in the literature and the tested model. Section V discusses the results obtained and the metric algorithm for validating detection and false alarms. Finally, section VI brings concluding remarks of the study.

Gabriel Luiz Espindola Pedro, Diego da Silva de Medeiros Arthur Cadore Matuella Barcella are with the Department of Telecommunications, Instituto Federal de Santa Catarina, São Jose-SC, e-mails: gabrielluizep.glep@gmail.com, diegomedeiros@ifsc.edu.br, arthurbarcella.cadore@gmail.com. Dimas Irion Alves and Paulo Ricardo Branco da Silva are with the Department of Telecommunications, Instituto Tecnológico da Aeronáutica, São José dos Campos-SP, e-mails: dimasirion@ita.br and pbranco@ita.br; João Vitor Rosa Negri is with the Department of Communications and Signal Processing, Universidade Federal de Santa Catarina, Florianópolis-SC, e-mail: joao.vitornegri@gmail.com. This work was partially sponsored by FINEP (01.22.0581.00), National Institute of Science and Technology (INCT-Signals) sponsored by Brazil's National Council for Scientific and Technological Development (CNPq) under grant no. 406517/2022-3, Ministry of Science, Technology and Innovation (MCTI), and by the São Paulo Research Foundation (FAPESP) under grant 20/09838-0 (BI0S—Brazilian Institute of Data Science).

II. Wavelength-Resolution SAR Images

Traditionally SAR systems uses microwave wavelengths to image the scenario [1]. This choice of frequency impacts directly the penetrability of the signal. In this sense, traditional SAR systems are not well suited for Foliage Penetration (FOPEN) applications, since smaller wavelengths suffers from back-scattering from small objects, thus leaves impacting substantially the reflected signal [1].

In the wavelength-resolution regime the spatial resolution of the SAR system is comparable to the wavelength of the transmitted signal, i.e., the distance between two distinguishable objects is in the order of the wavelength of the transmitted signal [1]. To emphasize the detection of larger targets, signals with longer wavelengths are used, i.e., signals with frequencies in the order of MHz.

This characteristic leads also to a minimization of speckle noise, since one resolution cell has at most one scatterer [3]. Also, due to the temporal characteristics of large targets, the images exhibit temporal stability, being a good candidate for CD [3].

Illustrating the concept of a wavelength-resolution system, the CARABAS-II is a Very High Frequency (VHF) Ultra-wideband (UWB) SAR system developed by the Swedish Defense Research Agency (FOI). Mounted on a Sabreliner aircraft, the system uses radio waves emitted from two phased wide-band dipoles with frequencies ranging from 20 to 90 MHz to create scene imagery [10]. The system features a cell resolution of 1×1 (one pixel per square meter) and a system resolution of approximately 2.5×2.5 (minimum detectable object size).

One of the core applications of the VHF SAR systems is FOPEN, in 2002 it was developed a flight campaign in Visdel, Sweden, which provided a dataset containing 24 images, each of them covering an area of 3 km $\times$ 2 km, containing 25 vehicles deployed on the forest that was imaged [5]. The images are divided in four deployments, each deployment containing six passes with three groups of two repeated flight headings. Figure 1 shows an example of image from the dataset, which can be found in [11].

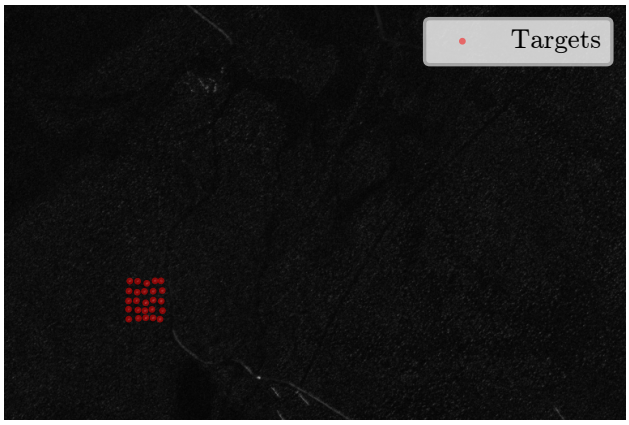

Fig. 1: An example image acquired during Mission 2, Pass 3 of the CARABAS-II campaign, with targets highlighted in red.

III. Change Detection Method

The CD method presented in this work employs Bayes' Theorem to compute the probability of pixel-level changes [6]. For each pixel, we evaluate the posterior probability $P(s \equiv s_T \mid z_s, z_r)$ of containing a target change ($s \equiv s_T$) given surveillance (z_s) and reference (z_r) image values as

$$P\left(s \equiv s_T | z_s, z_r\right) = \frac{P\left(z_s | s \equiv s_T, z_r\right) P\left(s \equiv s_T | z_r\right)}{P\left(z_s | z_r\right)}. \quad (1)$$

Applying the Bayes Theorem and the considerations made in [6], we achieve the equation that relates the probability of a pixel containing a target with the empirical values and the theoretical expected clutter values, defined as

$$P\left(s \equiv s_T \mid z_s, z_r\right) = \max\left(0,\ 1 - \frac{P\left(z_s, z_r \mid s \not\equiv s_T\right)}{P\left(z_s, z_r\right)}\right), \quad (2)$$

where $P(z_s, z_r \mid s \not\equiv s_T)$ represents the clutter-conditional probability and $P(z_s, z_r)$ denotes the total empirical probability. The $P(z_s, z_r \mid s \not\equiv s_T)$ derives from a bivariate distribution Probability Density Function (PDF), while the $P(z_s, z_r)$ term is estimated through histogram analysis of empirical pixel value co-occurrences.

It is expected that the histogram constructed from two images containing only clutter will closely match the shape of the theoretical distribution PDF. The addition of targets to the images results in higher observed values, which are not predicted by the PDF, leading to a mismatch between the histogram and the theoretical model. This discrepancy indicates a high probability of change obtained by (2).

Based on (2), we can describe the change detection method considered in this work, which consists, respectively, of obtaining the empirical histogram, calculating (2), detection based on a threshold, and a stage of morphological operations to exclude detections of objects with dimensions that do not fit the application. This method is represented in the simplified block diagram presented in Figure 2.

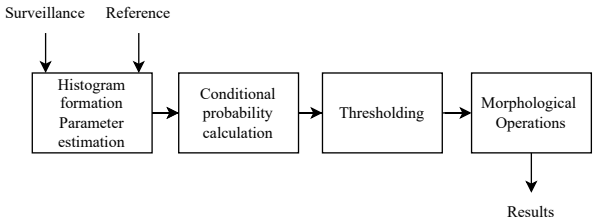

Fig. 2: Block diagram for noniterative algorithm, adapted from [6].

There are established models for the clutter-plus noise for wavelength-resolution SAR imagery, for example bivariate complex Normal distribution for complex images [7], bivariate Rayleigh distribution for magnitude images [12], bivariate Normal distribution for difference images [8] and bivariate

Gamma distribution for intensity difference images [9]. Based on the observed results, this work will evaluate the bivariate Normal, Rayleigh and Gamma distribution models.

A. Implementation Aspects

As the bivariate Gamma distribution is established as a model for clutter-plus-noise in intensity difference images, it is required to create this type of image from the combination of pairs, by subtracting two base images and squaring it [9]. For comparison, we used the same combinations provided in [9].

Knowing that large structures that also can reflect the transmitted signal are stable in time, we focus the analysis on appearing targets in the z_s, occurring only when $z_s \geq z_r$, and, to avoid small value fluctuations to be considered as valid cells to test, we add a guard value τ to test the cell only when $z_s >= z_r + \tau$, the same constraints are made in [8], [6], [12], [13]. This reduces computational effort and focuses the analysis on the distribution tail, where the targets are most likely localized, and the histogram matches the theoretical PDF more. For a fair comparison, we used the same values provided by literature $\tau \in \{0.2, 0.3, 0.4\}$.

To calculate the probability $P(z_s, z_r | s \neq s_T)$, we first need to estimate the shape k and scale θ parameters for the z_s and z_r images from the CD pair. For the parameter estimation, the Maximum Likelihood Estimator (MLE) was employed.

Subsequently, the association parameter η between the image pair can be calculated by

$$\eta = \begin{cases} \rho\sqrt{\dfrac{k_s}{k_r}} & \text{if } k_1 \geq k_2 \\ \rho\sqrt{\dfrac{k_r}{k_s}} & \text{if } k_1 < k_2 \end{cases}, \tag{3}$$

where ρ is the Pearson's product-moment correlation coefficient.

Based on this setup, the bivariate Gamma PDF can be computed to retrieve the likelihood of a pixel being clutter, given by

$$\begin{aligned} f(z_s, z_r) = {} & \frac{1}{\Gamma(k_r)\Gamma(k_s - k_r)\theta_s\theta_r(1-\eta)\eta^{(k_r-1)/2}} \\ & \times \left(\frac{z_s}{\theta_s}\right)^{k_s - k_r} \left(\frac{z_s}{\theta_s}\frac{z_r}{\theta_r}\right)^{(k_r-1)/2} \\ & \times \exp\left[-\frac{1}{1-\eta}\left(\frac{z_s}{\theta_s} + \frac{z_r}{\theta_r}\right)\right] \\ & \times \int_0^1 (1-t)^{(k_r-1)/2} t^{(k_s-k_r-1)} \\ & \times \exp\left[\frac{\eta}{1-\eta}\left(\frac{z_s}{\theta_s}\right)t\right] \\ & \times I_{k_r-1}\left[\frac{2}{1-\eta}\sqrt{\eta\left(\frac{z_s}{\theta_s}\frac{z_r}{\theta_r}\right)(1-t)}\right] dt, \end{aligned} \tag{4}$$

where $I_{(\cdot)}[\cdot]$ stands for the modified Bessel function of the first kind.

It is important to emphasize that the calculation of the bivariate Gamma PDF has an elevated processing cost due to the integral calculation with a Bessel function in the integrand. Therefore, τ plays an important role in reducing the amount of pixels that will be calculated, making the process quicker. As a result of the change detection method we are left with a bi-dimensional probability matrix, with each value in the matrix representing the likelihood of the corresponding pixel contains a target.

In order to define a detection, we must compare the value with a threshold λ. A detection is declared at a pixel if $P(s \equiv s_T | z_s, z_r) \geq \lambda$. To ensure consistency, we adopted values for $\lambda \in \{0.1, 0.2, 0.3, 0.4, 0.5, 0.6, 0.7, 0.8\}$, same as in [6].

For false alarm minimization, morphological operations are performed. By using erosion, we are able to eliminate small detections that did not represent actual targets, since the target dimensions are greater than the system resolution. The erosion process was followed by two dilation steps: first, a dilation using a 3×3 kernel—the same size as the one used for erosion—was applied to restore detections larger than 3 meters. Subsequently, a second dilation was performed with a 7×7 kernel, resulting in detected targets that represent areas of 10×10 meters.

To validate correct detections and false alarms, we compared the centroids of the detected objects with the ground truth positions from the deployment. A detection is considered correct if its centroid lies within 10 meters of any ground truth position, otherwise, it is classified as a false alarm. To ensure consistency, the literature models were also subjected to the same validation criteria. Algorithms 1 and 2 illustrates as a pseudo-code the step by step process for the change detection process and the detection and false alarm evaluation.

Algorithm 1: Detection process pseudo-code

Data: Interest image a; Reference image b; Subtraction base image c

Create the z_s and z_r images;
$z_s \leftarrow |a - c|^2$;
$z_r \leftarrow |b - c|^2$;
Create a 2D histogram with the values of z_s and z_r;
Estimate k_s k_r θ_s θ_r and η;
Create a mask for the pixels where $z_s \geq z_r + \tau$;
Create $P(z_s, z_r | s \neq s_T)$ with the PDF for the pixels within the mask;
Create $P(z_s, z_r)$ with the recurrence count for z_s and z_r values;
Create the target likelihood matrix P;
$P \leftarrow \max(0, 1 - P(z_s, z_r | s \neq s_T)/P(z_s, z_r))$;
Apply low-pass filter with kernel 3×3;
$P \leftarrow 0$ in the pixels where $(a - c) < 0$;
Create detections matrix D;
$C \leftarrow P > \lambda$;
Erode C with kernel 3×3;
Dilate C with kernel 3×3;
Dilate C with kernel 7×7;

Result: Binary change map C

Algorithm 2: Detection validation process pseudo-code

Data: Binary change map C
Data: Ground truth positions pixel list l
Identify objects from the connected pixels in C;
Find the centroids of each object;
Initialize false alarms and detection counters with 0;
for *each detected centroid* **do**
  if *the centroid position is in a 10 pixel radius of any ground truth* **then**
    Increment the detection counter;
    Delete ground truth position;
  else
    Increment false alarm counter;
  end
end
$P_d \leftarrow$ detection counter divided by 25;
$FAR \leftarrow$ false alarms counter divided by 6;
Result: Probability of detection P_d
Result: False alarm rate FAR

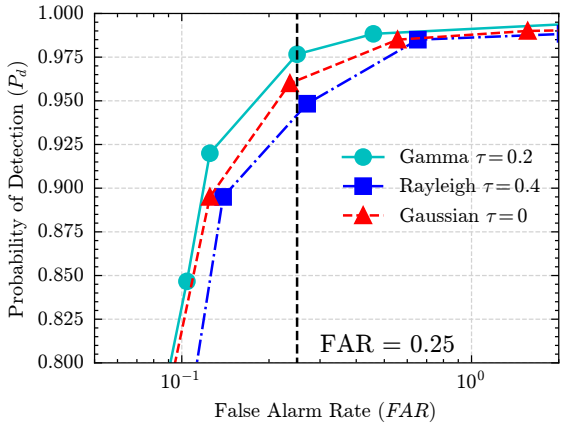

Fig. 3: ROC Curves comparing Gamma with literature models

IV. Results

This paper evaluates the performance of the proposed CD algorithm by analyzing Receiver Operating Characteristic (ROC) curves under different clutter models. As a comprehensive benchmark against other algorithms lies beyond the scope of this work, the analysis is restricted to variations in clutter modeling.

Figure 3 presents an ROC curve comparing the best results obtained for each model. The value $\tau = 0.2$ was selected for the bivariate Gamma due to its superior performance in the false alarm rate range of interest. For the bivariate Rayleigh, $\tau = 0.4$ was used as it provided the best overall result for that distribution. In the case of the bivariate Normal, $\tau = 0$ was chosen due to the lower complexity of its PDF and the good match with the histogram in the center region. Among all tested τ values, the bivariate Gamma distribution consistently achieves a higher Probability of Detection (P_d) than the other distributions under the same False Alarm Rate (FAR) scenario.

As is shown in Figure 3 an increase in the threshold λ reduces false alarms, concurrently limiting the detection. The CD image visual inspection confirms that behavior, Figure 4 shows the detection image for experiments 1 and 18 [9], for $\tau = 0.2$, $\lambda = 0.1$ and $\lambda = 0.3$.

TABLE I: P_d performance comparison for different clutter-plus-noise models at FAR $= 0.25/\text{km}^2$ and FAR $= 1.00/\text{km}^2$.

Model	τ	P_d [%]	
		$FAR = 0.25/km^2$	$FAR = 1/km^2$
Gamma	0.2	97.67	98.94
	0.3	97.42	-
	0.4	97.40	-
Gaussian	0.0	96.11	98.72
Rayleigh	0.4	93.99	98.58

As τ increases, the maximum FAR decreases, which leads to a smaller maximum point in the FAR axis for the curves with greater τ values. Considering this, we selected two operation points, one for the minimum FAR value between the maximum of each τ curve, $FAR = 0.25/\text{km}^2$, and one for the standard operation point in the literature, $FAR = 1/\text{km}^2$. Enabling the comparison among all τ values tested in this study and the standard used in the literature. Table I shows a comparison of P_d at the two chosen operation points for FAR. Obtaining the best result for the bivariate Gamma model with $\tau = 0.2$, with 97.67% and 98.94%, for FAR values of 0.25 and 1 per kilometer squared respectively.

V. Discussion

The bivariate Gamma model outperforms the other clutter models applied to the CD algorithm discussed in this paper. However, the model does not entirely capture all clutter behavior, as indicated by the use of τ, which limits the analysis to the tail of the distribution, where detection takes place.

The use of τ also reduced the number of tested pixels, directly impacting computational time. Given that the calculation of the PDF is computationally expensive, it is crucial to assess the operational applicability of this approach for time-sensitive applications. In the case of the Gamma distribution, τ tends to be highly selective, which helps reduce false alarms but can also lead to the removal of actual targets. Without applying τ, however, the system becomes computationally costly and prone to a large number of false positives due to distribution mismatch. Therefore, a compromise value of $\tau = 0.2$ was adopted. For the Rayleigh model, $\tau = 0.4$ was selected, as it yielded the best detection performance. Finally, for the Normal distribution, $\tau = 0$ was used both because of its simplicity and because it resulted in the best performance among the tested configurations.

As observed in Table I, as the values of τ decrease, P_d increases for a fixed value of FAR. This suggests that there is an optimal value of τ at which the maximum P_d can be achieved. In high FAR scenarios, potentially false alarms link one or more correctly detected targets. This event shifts the centroid of the detected object, which may result in a reduction in the number of detected targets. Also, if a false alarm links

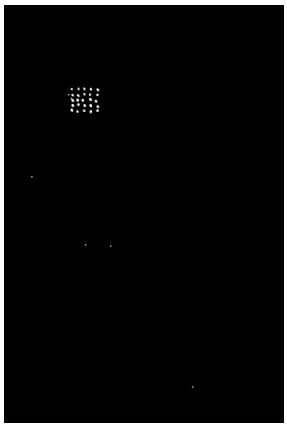

(a) Experiment 1, $\lambda = 0.1$

(b) Experiment 18, $\lambda = 0.1$

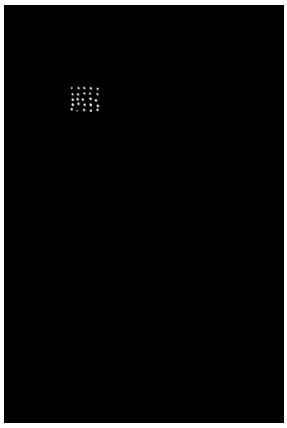

(c) Experiment 1, $\lambda = 0.3$

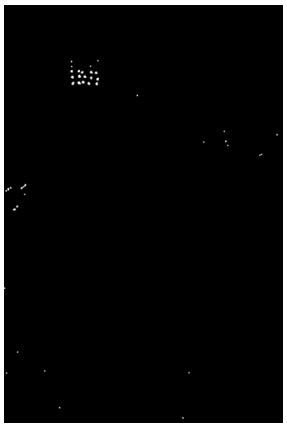

(d) Experiment 18, $\lambda = 0.3$

Fig. 4: Comparison of detection results for experiments 1 and 18 at thresholds $\lambda = 0.1$ and $\lambda = 0.3$ on clutter model bivariate Gamma distribution with $\tau = 0.2$.

two objects, that would count as correct detection, and the centroid remains within a radius of 10 pixels from the ground truth, the detection would count as one. Figure 5 illustrates this scenario. With that, a better detection validation method should be considered.

VI. Final Remarks

Overall, the bivariate Gamma distribution was shown to be more well-fitted to describe the tail behavior of the clutter, resulting in a reduction of false alarms when compared to the previously used in the literature. Reaching highers $P_d = 97.67\%$ for $FAR = 0.25/\text{km}^2$ and $P_d = 98.94\%$ for $FAR = 1/\text{km}^2$.

Although it achieved a superior P_d, it should be noticed that the bivariate Gamma distribution has an elevated computational cost due to the complexity of his PDF formula, and, differently from the bivariate Rayleigh distribution, it needs intensity difference images to serve as input for the method.

For future work, we will implement the iterative version of the change detection method to analyze the performance of

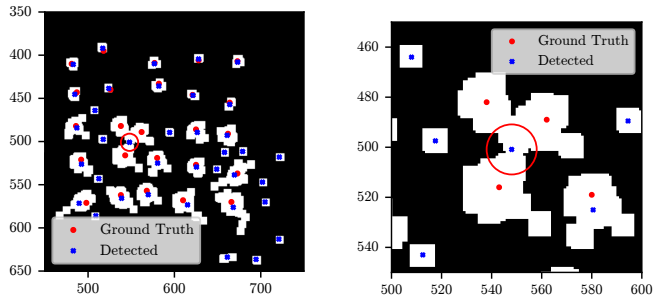

Fig. 5: Grouped detection example from experiment 18 using the Rayleigh model with $\tau = 0.4$.

P_d using the bivariate Gamma distribution as a clutter model. Additionally, a study on the effects of τ on the ROC curve is planned to evaluate the optimal point for maximizing the probability of detection.

References

[1] H. Hellsten, *Meter-wave synthetic aperture radar for concealed object detection*. Boston: Artech house, 2017.

[2] G. Smith, A. Persson, J. Hohmgren, B. Hallberg, J. Fransson, and L. Ulander, "Forest stem volume estimation using high-resolution lidar and SAR data," in *IEEE International Geoscience and Remote Sensing Symposium*, vol. 4, Jun. 2002, pp. 2084–2086 vol.4. [Online]. Available: https://ieeexplore.ieee.org/document/1026452

[3] R. Machado, V. T. Vu, M. I. Pettersson, P. Dammert, and H. Hellsten, "The Stability of UWB Low-Frequency SAR Images," *IEEE Geoscience and Remote Sensing Letters*, vol. 13, no. 8, pp. 1114–1118, Aug. 2016.

[4] C. Oliver and S. Quegan, *Understanding Synthetic Aperture Radar Images*. Raleigh, NC: SciTech Publishing, 2004.

[5] M. Lundberg, L. M. H. Ulander, W. E. Pierson, and A. Gustavsson, "A challenge problem for detection of targets in foliage," E. G. Zelnio and F. D. Garber, Eds., Orlando (Kissimmee), FL, May 2006.

[6] D. I. Alves, B. G. Palm, H. Hellsten, V. T. Vu, M. I. Pettersson, R. Machado, B. F. Uchôa-Filho, and P. Dammert, "Wavelength-Resolution SAR Change Detection Using Bayes' Theorem," *IEEE Journal of Selected Topics in Applied Earth Observations and Remote Sensing*, vol. 13, pp. 5560–5568, 2020.

[7] L. Ulander, M. Lundberg, W. Pierson, and A. Gustavsson, "Change detection for low-frequency SAR ground surveillance," *IEE Proceedings - Radar, Sonar and Navigation*, vol. 152, no. 6, p. 413, 2005.

[8] D. I. Alves, B. G. Palm, H. Hellsten, R. Machado, V. T. Vu, M. I. Pettersson, and P. Dammert, "Change Detection Method for Wavelength-Resolution SAR Images Based on Bayes' Theorem: An Iterative Approach," *IEEE Access*, vol. 11, pp. 84 734–84 743, 2023.

[9] G. H. Mittmann Voigt, D. Irion Alves, C. Müller, R. Machado, L. P. Ramos, V. T. Vu, and M. I. Pettersson, "A Statistical Analysis for Intensity Wavelength-Resolution SAR Difference Images," *Remote Sensing*, vol. 15, no. 9, p. 2401, Jan. 2023.

[10] H. Hellsten, L. M. H. Ulander, A. Gustavsson, and B. Larsson, "Development of VHF CARABAS II SAR," in *Radar Sensor Technology*, vol. 2747. SPIE, Jun. 1996, pp. 48–60.

[11] Air Force Research Laboratory, Sensors Directorate, "Vhf change detection problem set," https://www.sdms.afrl.af.mil/index.php?collection=vhf_change_detection. [Online]. Available: https://www.sdms.afrl.af.mil/index.php?collection=vhf_change_detection

[12] N. R. Gomes, M. I. Pettersson, V. T. Vu, P. Dammert, and H. Hellsten, "Likelihood ratio test for incoherent wavelength-resolution SAR change detection," in *2016 CIE International Conference on Radar (RADAR)*, Oct. 2016, pp. 1–4.

[13] V. T. Vu, N. R. Gomes, M. I. Pettersson, P. Dammert, and H. Hellsten, "Bivariate Gamma Distribution for Wavelength-Resolution SAR Change Detection," *IEEE Transactions on Geoscience and Remote Sensing*, vol. 57, no. 1, pp. 473–481, Jan. 2019.